P_n tomographic velocity and anisotropy beneath the Tibetan Plateau and the adjacent regions

Yan Lü[1], Sidao Ni[1,3], Bin Liu[1], and Youshun Sun[2]

[1]School of Earth and Space Sciences, University of Science and Technology of China, Hefei 230026, China
[2]Department of Earth, Atmospheric and Planetary Sciences, Massachusetts Institute of Technology, Cambridge, Massachusetts 02139, USA
[3]Key Laboratory of Dynamical Geodesy, Institute of Geodesy and Geophysics, Wuhan 430077, China

(Received April 9, 2011; Revised July 20, 2011; Accepted July 21, 2011; Online published February 14, 2012)

We present a tomographic velocity and anisotropy model of the uppermost mantle beneath the Tibetan Plateau and the adjacent regions. The investigation analyzed 105,385 P_n phase readings from the International Seismological Centre (ISC) and the China Earthquake Data Center. The average P_n velocity under the study area is approximately 8.15 km/s, with velocity perturbations up to 3–4%. We find high P_n velocities under the Indian Plate and in the Tarim and Sichuan basins, low P_n velocities under the Hindu Kush and in Myanmar and the adjacent region, and especially low P_n velocities under the area north of the Indus-Yarlung Zangbo suture. The high P_n velocity anomalies of the Indian Plate are discontinuous at the collision region in the east-west direction, indicating that the Indian Plate probably subducts in a piecewise manner. Distributions of P_n velocities are used to validate mechanisms for the subduction of the Indian Plate presented in previous studies. In addition, P_n anisotropy is obtained simultaneously with P_n velocity. At plate collision zones, the fast P_n anisotropy direction is parallel to the direction of the collision edge. We validate the existence of P_n anisotropy under these regions and discuss the relationship of anisotropy with tectonic structure and plate movement.

Key words: P_n velocity, anisotropy, Indian Plate, Tibetan Plateau.

1. Introduction

The Tibetan Plateau and the adjacent regions include China's Tarim Basin, the Sichuan-Yunnan region, and Afghanistan, India, Myanmar and other neighboring countries (Fig. 1). The tectonics of the area is currently controlled by the collision and continuing convergence of the Indian Plate and the Eurasian plates. This collision is a very important continent-continent collision zone, as it dominantly affects the regional structure and geology (Molnar and Tapponnier, 1975). The northward movement of the Indian Plate has been widely accepted as the driving force for growth of the Tibetan Plateau; however, the mechanism of subduction is still unclear and requires further examination.

In the uppermost mantle, changes in composition, temperature, pressure and water volatile content contribute to P_n velocity variations. The preferred alignment of olivine crystals, caused by the creeping of material in the uppermost mantle, is believed to contribute to P_n velocity anisotropy (Ribe, 1992). Thus, P_n velocity variations and anisotropy provide constraints on the processes of continental deformation and differentiation.

This region has been studied in the past by various authors (e.g., Kind *et al.*, 2002; Liang *et al.*, 2004, 2006; Sun and Toksöz, 2006; Pei *et al.*, 2007; Phillips *et al.*, 2007; Zheng *et al.*, 2007; Sun *et al.*, 2008). In these studies, high P_n velocities have been discovered beneath the Indian Plate and low velocities have been found in the eastern India and Myanmar regions. P_n anisotropy models have also been developed by previous studies. However, advances in tomography technology have led to a denser seismic ray path coverage than those in earlier studies. Here, we present improved P_n velocity and anisotropy tomographic models of the uppermost mantle beneath the Tibetan Plateau and the adjacent regions using both seismic data from the Chinese Earthquake Network catalogs and data from the ISC catalogs. This new dataset contains P_n arrival readings from stations in both India and China, thus providing tighter constraints on the velocity structure near the India-China border. These high-resolution data are very useful for the investigation of the complex tectonics of this region. The distributions of P_n velocities and anisotropy provide some hypotheses on the subduction mechanisms of the Indian Plate.

2. Data and Method

Our study area is situated between 20°N and 40°N in latitude, and 65°E and 105°E in longitude. Seismic data from 4319 events recorded by 296 stations between 5°N and 55°N, and 50°E and 120°E are used in the study. These data are from events occurring between 1990 and 2009 in the Chinese seismic network and from 1960 to 2007 in the ISC catalogs. Figure 2 shows the source-station ray paths for the study area.

For the inversion, we used P_n data for which the epicenter distance range was between 2° and 12°. We chose the lower limit of 2° to remove the P_g phases and the upper limit of

doi:10.5047/eps.2011.07.013

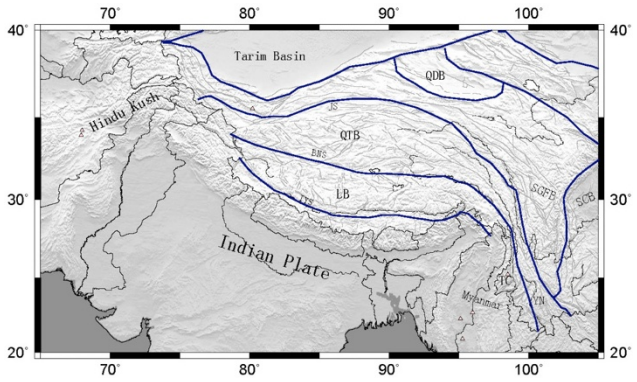

Fig. 1. Simplified tectonic map of the Tibetan Plateau and the adjacent regions superimposed on topography. BNS: Bangong-Nujiang suture, IYS: Indus-Yarlung Zangbo suture, JS: Jinsha River suture, LB: Lhasa Block, QDB: Qaidam Basin, QTB: Qiangtang Block, SCB: Sichuan Basin, SGFB: Songpan-Ganzi fold belt, TC: Tengchong Volcano, YN: Yunnan. Triangles denote volcanoes.

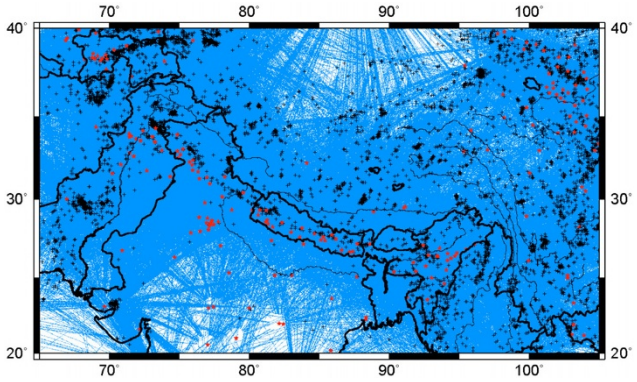

Fig. 2. Ray paths for P_n traveltimes. From 4319 events recorded by 296 stations, 105,385 P_n rays were obtained. Events are represented by black crosses and stations are indicated by red stars.

12° to include only the observations along the linear portion of the travel time curve, as well as to avoid arrivals from the deeper part of the upper mantle. Within this distance range, the P_n phases are the first arrivals. The initial models were obtained by a linear fit to the traveltime-distance curve. The traveltime residuals to the fitted line used in this paper are limited to a range of ±6 s. Using this methodology, 105,385 P_n rays were obtained.

We followed the P_n tomography method developed by Hearn (1996). The uppermost layer of the mantle is divided into a set of two-dimensional cells in which the slownesses (the inverse of velocities) are to be inverted. The P_n traveltime residuals are described approximately by the perturbation equation

$$t_{ij} = a_i + b_j + \sum d_{ijk}(S_k + A_k \cos 2\phi_{ijk} + B_k \sin 2\phi_{ijk}), \quad (1)$$

where t_{ij} is the traveltime residual for event j and station i, a_i is the static delay for station i, b_j is the static delay for event j, d_{ijk} is the travel distance of ray ij in mantle cell k, S_k is the slowness perturbation for cell k, A_k and B_k are the anisotropy coefficients for cell k, and ϕ_{ijk} is the back azimuth angle of the ray ij at cell k. The magnitude of the anisotropy is given by $\sqrt{A_k^2 + B_k^2}$, and the direction of the fastest wave propagation is given by $90^\circ + \frac{1}{2}\arctan\frac{B_k}{A_k}$. The unknown quantities in Eq. (1) are the mantle slowness perturbation S_k, anisotropy parameters A_k and B_k, and the station and event delays a_i and b_j, respectively. For P_n waves, the station and event delays accommodate variations in crustal velocity and thickness; the slowness variations are unaffected by the crust and reflect only the variations in mantle velocity. In solving the set of traveltime equations, we used a cell size of $20' \times 20'$. The slowness values in each cell were iteratively resolved by the LSQR algorithm (Paige and Saunders, 1982; Yao *et al.*, 1999). In the inversion, two damping constants were used: one controls the smoothness of the velocity image by damping the variations in slowness, and the other controls the smoothness of the anisotropy by damping the two anisotropy coefficients. These two damping constants were assumed to be equal, which is also adopted in studies by Hearn (1999) and Pei *et al.* (2007). Figure 3 shows that the standard deviation of P_n traveltime residuals decreased from 2.0 s to 1.1 s after the inversion. For comparison, we also studied P_n velocity models without the anisotropy effects.

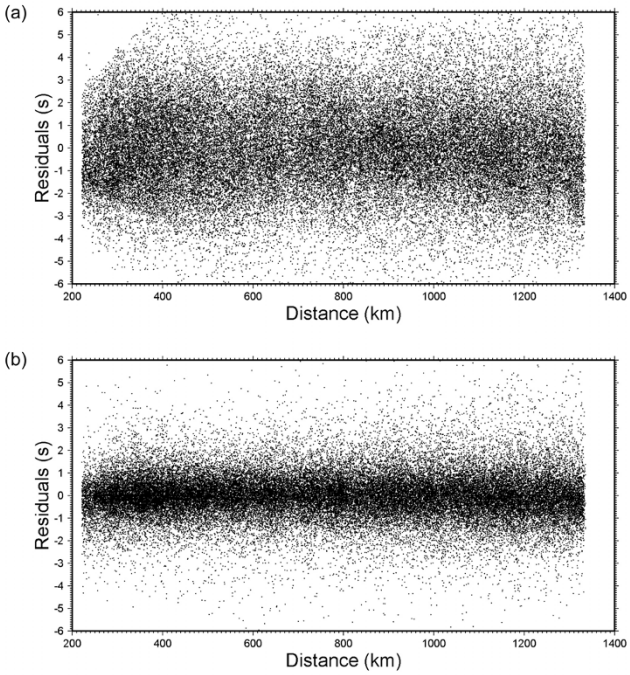

Fig. 3. Distribution of residuals versus epicentral distance before inversion (a) and after joint velocity and anisotropy inversion (b). The standard deviation of P_n traveltime residuals is 2.0 s for the original data and decreases to 1.1 s after inversion.

3. Checkerboard Test

Checkerboard tests were conducted to evaluate how ray coverage affects the spatial resolution of our tomography study. A test checkerboard velocity model was created by simultaneously assigning both sinusoidal velocity and anisotropy anomalies to the cells of the model domain. Synthetic arrival times were calculated for the test model for different checkerboard sizes of velocity and anisotropy with the same number of earthquakes, stations and ray paths as

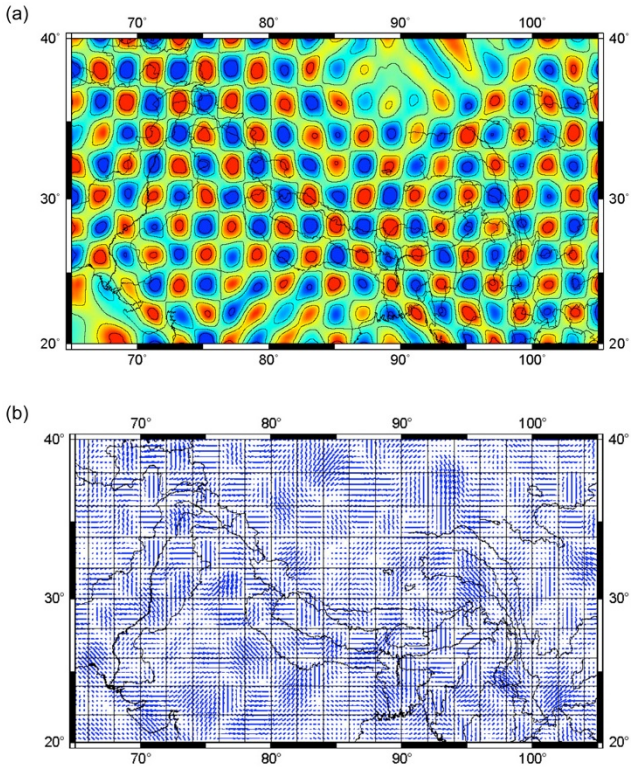

Fig. 4. Checkerboard test result for velocity (a) and anisotropy (b). Checkerboard size is 2.0° × 2.0° for velocity and anisotropy. The isopleths in Fig. 4(a) are pointing −0.3, −0.15, 0.0, 0.15 and 0.3 km/s velocity anomaly.

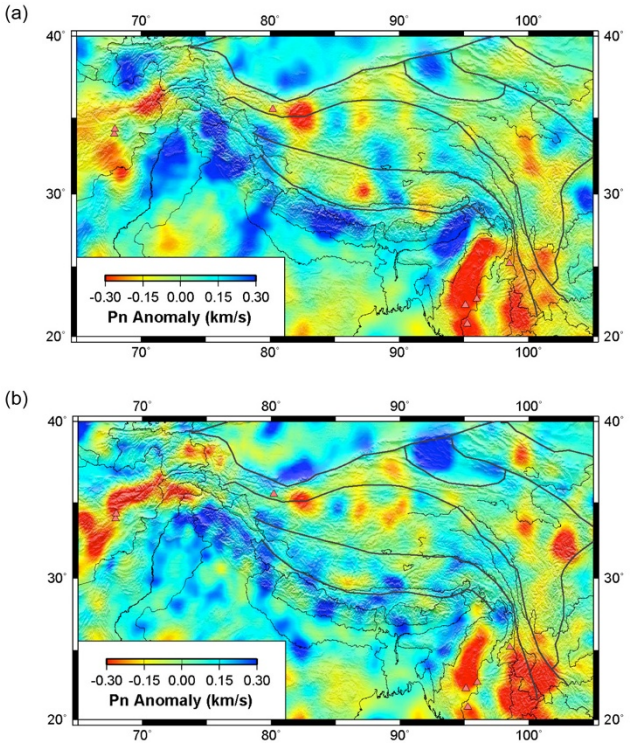

Fig. 5. P_n lateral velocity variations with anisotropy (a) and without anisotropy (b). The average P_n velocity is 8.15 km/s. Red and blue areas correspond to velocities lower and higher than the average, respectively. Triangles denote volcanoes.

those used for tomographic inversion of the real data. As we conservatively assume that traveltime residuals after inversion consist of pick errors, source/station uncertainties, and other noises, we added Gaussian noise, with a standard deviation of 1.1 s, to the synthetic traveltimes. The average amplitude ($\max\Delta v/\sqrt{2}$) of the sinusoidal velocity and anisotropy anomalies is 0.30 km/s. We tested different sizes of sinusoids for velocity and anisotropy. The tests indicate that for most of the Iranian region, 2.0° × 2.0° cells for P_n velocity and anisotropy can be resolved well (Fig. 4). The spatial resolution is considered to be good for the regions in which the checkerboard pattern is recovered. In addition, the obtained resolution is higher than in previous studies.

4. Results and Discussion

Figure 5(a) shows the P_n velocity variations with the anisotropy effects. The average P_n velocity under the study area is approximately 8.15 km/s, with maximum velocity perturbations of approximately 3–4%. In general, high P_n velocities were found under the Indian Plate and in the Tarim and Sichuan basins. Low P_n velocities were found under Myanmar, its adjacent region and in the Hindu Kush region. An especially low P_n velocity value was found under the area north of the Indus-Yarlung Zangbo suture (IYS).

The Indian Plate, which is subducting under Myanmar and the adjacent region from the southwest, displays obvious low P_n velocities. This is strong evidence for the existence of the upwelling of hot material caused by the subduction. These low-velocity anomalies are associated with volcanic activity, i.e., the Tengchong volcano, and is likely a result of the higher temperatures and/or partial melting associated with volcanism (Hearn and Ni, 1994). Low P_n velocity anomalies are also associated with the subduction in the Hindu Kush region as well. Here, the low velocity anomaly does not totally align with the volcanoes, but the distance between the volcanoes and the low velocity anomaly is not very large. The misalignment between the low velocity anomaly and the volcano distribution proba-

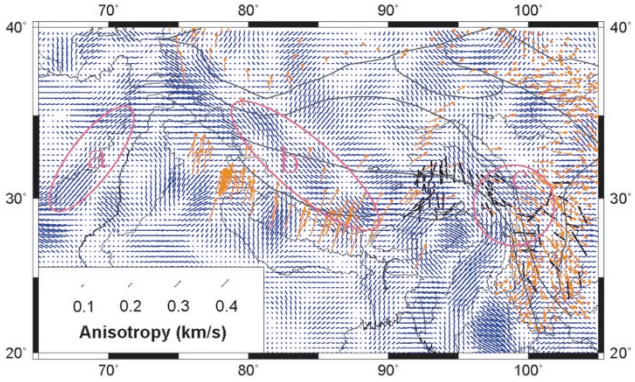

Fig. 6. Tomographic image of P_n velocity anisotropy. Blue line segments are drawn parallel to the direction of anisotropy, with their lengths proportional to the magnitude of anisotropy. Regions exhibiting large anisotropy and having dense ray coverage are marked with purple circles and labeled a, b, and c. The orange arrows represent crustal movement directions from GPS (Zhang *et al.*, 2004). The black lines represent the shear-wave splitting measurements (Sol *et al.*, 2007).

bly underscores the complexity of the crust at this region. Therefore, determining the detailed crustal structure from 3D tomography may help to illuminate the link between the volcanoes and the crustal velocity anomalies. It is widely accepted that the Indian Plate collided with the Asian Plate in the Tibetan Plateau, but the mechanism of subduction is still unclear. The cold lithosphere of the Indian Plate has a high P_n velocity, and this is confirmed in our inversion results. This high-velocity anomaly area roughly reaches the IYS. In the area north of the IYS suture, low P_n velocities were found. Zheng *et al*. (2007) proposed a model using teleseismic *P*-waves that the lithosphere of the Indian Plate subducted 200–300 km deep into the mantle. Our inversion results also support the theory that the lithosphere of the Indian Plate subducted into the mantle, causing the upwelling of hot material in the north of the IYS. In addition, the stable regions such as the Tarim and Sichuan basins have high P_n velocities, and the P_n velocity under the Songpan-Ganzi fold belt is significantly lower. The slow anomalies in the Yunnan-Myanmar region, the western part of the QTB and the Songpan-Ganzi fold belt, as well as the fast anomalies in the Tarim and Sichuan basins are consistent with previous studies (Liang *et al*., 2004; Pei *et al*., 2007). Our results also show that high P_n velocity anomalies in the Indian Plate are discontinuous at the collision region in the east-west direction, which suggests that the Indian Plate may subduct by different blocks. That is, the Indian plate probably does not subduct in one piece beneath Tibet, but rather in a piecewise manner. Liang *et al*. (2006) has also proposed that the Indian lithosphere advances northward in different pieces with different rates. As this discontinuous model may be affected by the uneven distribution of the ray paths or the trade-off between velocity and anisotropy, we believe that this conjecture demands more studies before confirmation.

We also obtained P_n velocities without the anisotropy effects for comparison (Fig. 5(b)). Both models share the following common features throughout most of the study area: high P_n velocities under the Indian Plate and in the Tarim basin, low P_n velocities under the Hindu Kush and in Myanmar and the adjacent region. We have also observed that the high P_n velocities in the Sichuan and Tarim basins are not as obvious as in the anisotropy model. Joint inversion with anisotropy helps to determine a more reliable velocity picture.

The P_n velocity anisotropy we obtained is shown in Fig. 6. Regions exhibiting large anisotropy and possessing dense ray coverage are marked with yellow circles and labeled as a, b, and c. We focus our discussion on these three regions. At the collision region between the Indian Plate and the Eurasian Plate (region a), the fast P_n anisotropy direction is NE-SW. At the collision region between the Indian Plate and the Tibetan Plateau (region b), the fast P_n anisotropy direction is NWW-SEE, which is parallel to the collision arc. The shear strains along the plate boundary may be responsible for the anisotropy there, since the shear traction on the base of the lithosphere could orient the olivine crystals' fast axes parallel to the shear direction (Ribe, 1992). In eastern Tibet (region c), the fast P_n anisotropy direction is NWW-SEE, as is the region's crustal movement direction. This result suggests that the preferred alignment of the olivine crystals is parallel to the direction of plate movement. Compared with those of previous studies (Liang *et al*., 2004; Pei *et al*., 2007), our P_n anisotropy results in the regions b and c are similar, suggesting that this anisotropic model is reliable. Our study provides better coverage in the study region, as previous studies do not have adequate ray path coverage due to fewer stations and events. Recent studies involving the comparison between GPS-observed plate motion and seismologically-observed anisotropy also support this idea (Xiong *et al*., 2003; Zhang *et al*., 2004; Wang *et al*., 2008). Shear-wave splitting measurement (Iidaka and Niu, 2001; Sol *et al*., 2007; Chen *et al*., 2010) was also compared with the P_n anisotropy. In region c, the fast direction of P_n anisotropy is generally the same as the *SKS* splitting fast direction. This suggests that the material flow at the uppermost mantle is coupled with the deeper parts. Around 93°E, the fast P_n direction is different from the *SKS* splitting fast direction, which might be caused by the eastward movement of the lithosphere due to the push from the collision and decoupling with the deep upper mantle.

5. Conclusions

We present high-resolution P_n velocity and anisotropy models for the uppermost mantle beneath the Tibetan Plateau and the adjacent regions using large data sets and provide constraints on plate structure and the processes of continental deformation. The average P_n velocity under the study area is approximately 8.15 km/s, with maximum velocity perturbations of approximately 3–4%. We found high P_n velocities beneath the Indian Plate and in the Tarim and the Sichuan basins, low P_n velocities under Myanmar, its adjacent region and the Hindu Kush region, and especially low P_n velocities under the area north of the IYS. The cold lithosphere in the Indian Plate exhibits a high P_n velocity. The high P_n velocity anomalies of the Indian Plate are discontinuous at the collision region in the east-west direction, which may be related to the block subduction process of the Indian Plate, indicating that the Indian plate probably subducts in a piecewise manner. In the area north of the IYS, low P_n velocities are associated with the subduction of the Indian lithosphere. The regions that are stable and less affected by tectonic activities, such as the Tarim and Sichuan basins, have high P_n velocities, and the P_n velocity under the Songpan-Ganzi fold belt is significantly lower. At the plate collisions, the fast P_n anisotropy direction is parallel to the collision arc. The anisotropy at the plate boundary may be caused by shear strains along the boundary; the shear traction on the base of the lithosphere could orient the fast axis in olivine crystals parallel to the shear direction. The fast P_n anisotropy in the eastern Tibetan Plateau suggests that the preferred alignment of olivine crystals is parallel to the plate movement direction.

Our results agree well with previous models but provide a more detailed uppermost mantle structure in the study area. In the near future, we expect to further enhance the regional model by developing an S_n model to delineate structural details around the low velocity zones.

However, P_n and S_n models only provide information of the uppermost mantle and therefore offer limited informa-

tion for crustal structures. Full 3D crustal P and S velocity models will definitely help to link surface geological features with tectonic processes at depth. With many more broadband seismic stations becoming available in Tibet and the adjacent regions, the recently-developed ambient noise tomography will help to provide more accurately-resolved crustal structures using short period surface waves as well as Moho-reflected body waves such as S_mS (Yang *et al.*, 2010; Zhan *et al.*, 2010).

Acknowledgments. We would like to thank Thomas M. Hearn for providing the original tomographic idea and codes. We thank Dr. Pei Shunping for his valuable comments. We also appreciate the insightful suggestions by two reviewers. The data from the Chinese Earthquake Network catalog are downloaded from http://www.csndmc.ac.cn, and the ISC data from http://www.isc.ac.uk. This study is supported by the National Nature Science Foundation of China (Grant No. 41074031 and 40940021) and China Earthquake Program 200808078.

References

Chen, W.-P., M. Martin, T.-L. Tseng, R. L. Nowack, S.-H. Hung, and B.-S. Huang, Shear-wave birefringence and current configuration of converging lithosphere under Tibet, *Earth. Planet. Sci. Lett.*, **295**(1–2), 297–304, doi:10.1016/j.epsl.2010.04.017, 2010.

Hearn, T. M., Anisotropic Pn tomography in the western United States, *J. Geophys. Res.*, **101**, 8403–8414, 1996.

Hearn, T. M. and J. Ni, Pn velocities beneath continental collision zones, the Turkish-Iranian Plateau, *Geophys. J. Int.*, **117**, 273–283, 1994.

Hearn, T. M., Uppermost mantle velocities and anisotropy beneath Europe, *J. Geophys. Res.*, **104**(B7), 15123–15139, 1999.

Iidaka, T. and F. Niu, Mantle and crust anisotropy in the eastern China region inferred from waveform splitting of SKS and PpSms, *Earth Planets Space*, **53**(3), 159–168, 2001.

Kind, R., X. Yuan, J. Saul, D. Nelson, S. V. Sobolev, J. Mechie, W. Zhao, G. Kosarev, J. Ni, U. Achauer, and M. Jiang, Seismic images of crust and upper mantle beneath Tibet: Evidence for Eurasian plate subduction, *Science*, **298**, 1219–1221, 2002.

Liang, C., X. Song, and J. Huang, Tomographic inversion of Pn travel times in China, *J. Geophys. Res.*, **109**, B11304, doi:10.1029/2003JB002789, 2004.

Liang, C., X. Song, and J. Huang, A low velocity belt beneath northern and eastern Tibetan Plateau from Pn tomography, *Geophys. Res. Lett.*, **33**, L22306, doi:10.1029/2006GL027926, 2006.

Molnar, P. and P. Tapponnier, Cenozoic tectonics of Asia: Effects of a continental collision, *Science*, **189**, 419–426, 1975.

Paige, C. C. and M. A. Saunders, LSQR, An algorithm for sparse linear equations and sparse linear system, *ACM Trans. Math. Software*, **8**, 43–71, 1982.

Pei, S., J. Zhao, Y. Sun, Z. Xu, S. Wang, H. Liu, C. A. Rowe, M. Nafi Toksöz, and X. Gao, Upper mantle seismic velocities and anisotropy in China determined through Pn and Sn tomography, *J. Geophys. Res.*, **112**, B05312, doi:10.1029/2006JB004409, 2007.

Phillips, W. S., M. L. Begnaud, C. A. Rowe, L. K. Steck, S. C. Myers, M. E. Pasyanos, and S. Ballard, Accounting for lateral variations of the upper mantle gradient in Pn tomography studies, *Geophys. Res. Lett.*, **34**, L14312, doi:10.1029/2007GL029338, 2007.

Ribe, N., On the relation between seismic anosotropy and finite strain, *J. Geophys. Res.*, **97**, 8737–8747, 1992.

Sol, S., A. Meltzer, R. Burgmann, R. D. van der Hilst *et al.*, Geodynamics of southeastern Tibet from seismic anisotropy and geodesy, *Geology*, **35**, 563–566, doi: 10.1130/G23408A.1, 2007.

Sun, Y. and M. N. Toksöz, Crustal structure of China and surrounding regions from P wave traveltime tomography, *J. Geophys. Res.*, **111**, B03310, doi:10.1029/2005JB003962, 2006.

Sun, Y., M. N. Toksöz, S. Pei, D. Zhao, F. D. Morgan, and A. Rosca, S-wave tomography of the crust and uppermost mantle in China, *J. Geophys. Res.*, **113**, B11307, doi:10.1029/2008JB005836, 2008.

Wang, C.-Y., L. M. Flesch, P. G. Silver, L.-J. Chang, and W. W. Chan, Evidence for mechanically coupled lithosphere in central Asia and resulting implications, *Geology*, **36**, 363–366, 2008.

Xiong, X., P.-H. Park, Y. Zheng, H. Hsu, and U. Han, Present-day slip-rate of Altyn Tagh Fault: Numerical result constrained by GPS data, *Earth Planets Space*, **55**(8), 509–514, 2003.

Yang, Y. *et al.*, Rayleigh wave phase velocity maps of Tibet and the surrounding regions from ambient seismic noise tomography, *Geochem. Geophys. Geosyst.*, **11**, Q08010, doi:10.1029/2010GC003119, 2010.

Yao, Z. S., R. G. Roberts, and A. Tryggvason, Calculating resolution and covariance matrices for seismic tomography with the LSQR method, *Geophys. J. Int.*, **138**, 886–894, 1999.

Zhan, Z., S. Ni, D. Helmberger, and R. Clayton, Retrieval of Moho reflected shear wave arrivals from ambient seismic noise, *Geophys. J. Int.*, **182**, 408–420, 2010.

Zhang, P., Z. Shen, M. Wang, W. Gan, R. Bürgmann, P. Molnar, Q. Wang, Z. Niu, J. Sun, J. Wu, H. Sun, and X. You, Continuous deformation of the Tibetan Plateau from global positioning system data, *Geology*, **32**, 809–812, 2004.

Zheng, H. W., T. D. Li, R. Gao, D. Zhao, and R. He, Teleseismic P-wave tomography evidence for the Indian lithospheric mantle subducting northward beneath the Qiangtang terrane, *Chinese J. Geophys.*, **50**(5), 1418–1426, 2007 (in Chinese).

Y. Lü (e-mail: lvyan@mail.ustc.edu.cn), S. Ni, B. Liu, and Y. Sun